JACS
JOURNAL OF THE AMERICAN CHEMICAL SOCIETY

Subscriber access provided by American Chemical Society

Article

# Computational Study on the Origin of the Stereoselectivity for the Photochemical Denitrogenation of Diazabicycloheptene

Adalgisa Sinicropi, Chris S. Page, Waldemar Adam, and Massimo Olivucci

*J. Am. Chem. Soc.*, **2003**, 125 (36), 10947-10959• DOI: 10.1021/ja0263137 • Publication Date (Web): 15 August 2003

**Downloaded from http://pubs.acs.org on March 29, 2009**

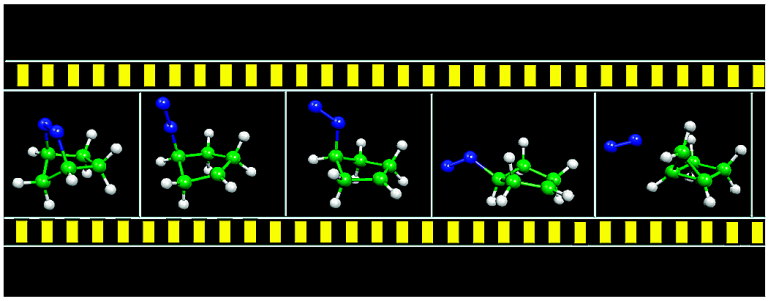

## More About This Article

Additional resources and features associated with this article are available within the HTML version:

- Supporting Information
- Access to high resolution figures
- Links to articles and content related to this article
- Copyright permission to reproduce figures and/or text from this article

View the Full Text HTML

ACS Publications
High quality. High impact.

Journal of the American Chemical Society is published by the American Chemical Society. 1155 Sixteenth Street N.W., Washington, DC 20036

J|A|C|S
ARTICLES
Published on Web 08/15/2003

# Computational Study on the Origin of the Stereoselectivity for the Photochemical Denitrogenation of Diazabicycloheptene

Adalgisa Sinicropi,[†] Chris S. Page,[†] Waldemar Adam,*[,‡] and Massimo Olivucci*[,†,§]

*Contribution from the Dipartimento di Chimica, Università di Siena, Via Aldo Moro, Siena, I-53100 Italy, Centro per lo Studio dei Sistemi Complessi, Via Tommaso Pendola 37, Siena I-53100 Italy, and Institut für Organische Chemie, Universitat Würzburg, Am Hubland, D-97074 Würzburg, Germany*

Received March 25, 2002; E-mail: olivucci@unisi.it

***Abstract:*** The origin of the inversion stereoselectivity of housane formation via *photochemical* nitrogen extrusion of diazabicycloheptene (**DBH**) has been investigated using reaction path computations and multireference second-order perturbation theory within a CASPT2//CASSCF scheme. We show that the primary photoproduct of the reaction is an *exo-axial* conformer of the diazenyl diradical (**$^1$DZ**) which displays a cyclopenta-1,3-diyl moiety with a *Cs*-like structure. **$^1$DZ** is selectively generated via decay at a *linear*−*axial* conical intersection, and it is located in a shallow region of the ground state potential energy surface that provides access to five different reaction pathways. Reaction path analysis (including probing with classical trajectories) indicates that production of inverted housane can only occur via *impulsive* population of an axial-to-equatorial pathway, and it is thus inconsistent with thermal equilibration of the primary **$^1$DZ** conformer. Similarly, according to the same analysis, the decrease of inversion stereoselectivity and even the retention (stereochemical memory effect) observed for suitably substituted **DBH**s are explained by dynamics effects where the axial-to-equatorial impulsive motion is restrained by the inertia and/or steric hindrance of the substituents. These results shade light on the poorly understood mechanisms that allow a photochemical reaction, in which a large amount of energy is deposited in the reactant by photon absorption, to show a high degree of stereoselectivity.

## 1. Introduction

During the last three decades, the bicyclic azoalkane diazabicyclo[2.2.1]heptene (**DBH**) has attracted much attention, especially because of the unusual stereoselectivity observed during both thermal and photochemical nitrogen extrusions. Indeed, nitrogen extrusion from the *exo*-deuterated parent system (***$d_2$*-DBH**) yields the inverted *exo*-deuterated bicyclo[2.1.0]-pentane (*exo* housane) as the major product.[1,2] The origin of the *thermal* stereoselectivity has been recently investigated by ab initio CASSCF and CASPT2 quantum chemical computations.[3] The authors have provided evidence in favor of a reaction mechanism that corresponds to a synchronous concerted denitrogenation process, in which both C−N bonds break simultaneously. Comparison of the symmetric $C_s$ reactant and transition structures indicates that a cyclopentane-1,3-diyl ring-inversion mode must be impulsively populated, after passage through the transition state. The observed prevalence of the inverted stereoisomer of the housane product may, thus, be explained in terms of a dynamic model, in which a puckered cyclopentane-1,3-diyl diradical (**$^1$DR**) precursor to the *inverted* housane (Allred-Smith model[4]) is formed preferentially or a nonstatistical **$^1$DR** intervenes, with an excited vibrational mode to generate *inverted* housane (Carpenter model[3]). These models are presently the only ones to provide an explanation for the fact that the observed inversion stereoselectivity is not consistent with the lowest-energy $C_2$-*symmetric* equilibrium structure of **$^1$DR**.[5]

The origin of the inversion stereoselectivity for the *photochemical* nitrogen extrusion[2] has not been computationally investigated at the same detailed level as the thermal process[3] and remains substantially unknown. Furthermore, the fact that a photochemical reaction, in which a large amount of energy is deposited in the reactant by photon absorption, could show a high degree of stereoselectivity at all is mechanistically poorly understood. For these reasons, we present here the results of an extensive computational investigation with multireference perturbation theory of the *singlet* reaction paths for the photochemical denitrogenation of the parent **DBH** to the corresponding housane.

Few years ago, we reported a computational study on the photochemical reactivity of **DBH.**[6] We found that the singlet pathway for nitrogen loss involves the excited state ($^1$n-$\pi^*$) cleavage of one C−N bond (Figure 1). The corresponding

[†] Dipartimento di Chimica, Università di Siena.
[‡] Centro per lo Studio dei Sistemi Complessi.
[§] Institut für Organische Chemie, Universitat Würzburg.

(1) Roth, W. R.; Martin, M. *Tetrahedron Lett.* **1967**, *47*, 4695−4698.
(2) Roth, W. R.; Martin, M. *Liebigs Ann. Chem.* **1967**, *702*, 1−5.
(3) Reyes, M. B.; Carpenter, B. K. *J. Am. Chem. Soc.* **2000**, *122*, 10 163−10 176.
(4) Allred, E. L.; Smith, R. L. *J. Am. Chem. Soc.* **1967**, *89*, 7133−7134.
(5) Sherrill, C. D.; Seidl, E. T.; III, H. F. Schaefer *J. Phys. Chem.* **1992**, *96*, 3712−3716.
(6) Yamamoto, N.; Olivucci, M.; Celani, P.; Bernardi, F.; Robb, M. A. *J. Am. Chem. Soc.* **1998**, *120*, 2391−2407.

10.1021/ja0263137 CCC: $25.00 © 2003 American Chemical Society

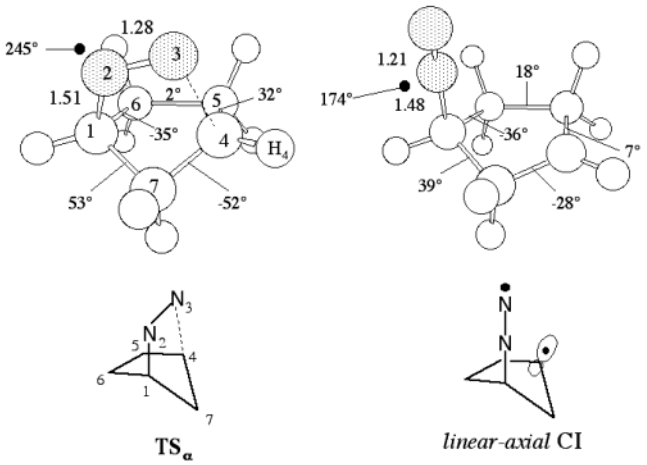


***Figure 1.*** Computed[6] transition structure (**TS**$_\alpha$) for the photochemical α cleavage of the azoalkane DBH and the *linear-axial* geometry within the conical intersection (**CI**).

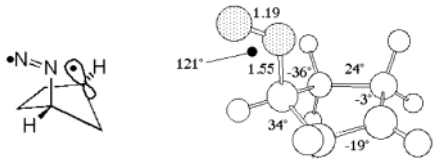


***Figure 2.*** Computed geometry for the *exo-axial* singlet diazenyl diradical (**$^1$DZ**); the radical center at the CH position is pyramidalized with the radical lobe directed toward the diazenyl functionality.

transition state (see structure **TS**$_\alpha$) connects the $^1$n-$\pi$* **DBH** equilibrium structure to a low-lying conical intersection between the excited- and ground-state potential energy surfaces.[7] Inspection of the structure of the conical intersection, the *linear-axial* **CI**, reveals that one C−N bond is still intact (1.48 Å), which suggests that relaxation to the ground state would lead to a singlet diazenyl-diradical intermediate (**$^1$DZ**). Although a **$^1$DZ** species has not been isolated, detected spectroscopically or trapped, its intervention as intermediate has also been suggested by various experimental facts.[8−10] In Scheme 1, we show the competing pathways that have been postulated to explain the stereochemistry for the photochemical denitrogenation of the **DBH**, with **$^1$DZ** as the common key intermediate. The $S_H2$ process involves the concerted backside displacement (analogous to the $S_N2$ mechanism) of the nitrogen molecule by the carbon-radical site and affords the inverted *exo* housane exclusively. In competition, the **$^1$DZ** diradical follows a denitrogenation pathway to the thermally equilibrated *$C_2$-symmetric* **$^1$DR** intermediate,[11] which collapses to both the retained and the inverted housanes in equal amounts and, thus, complete loss of stereoselectivity ensues. Finally, a third possible pathway is the one to produce retained housane. This pathway is associated with a stereochemical memory effect that has been observed in the confined space of a crystal lattice[12] and, very recently, for the first time in the liquid-phase photolysis of bridgehead substituted **DBH** derivatives.[10]

***Scheme 1.*** Alternative Mechanistic Pathways for the Photochemical Denitrogenation of the Azoalkane DBH through the Singlet Diazenyl ($^1$DZ) and the Cyclopentane-1,3-diyl ($^1$DR) Diradicals

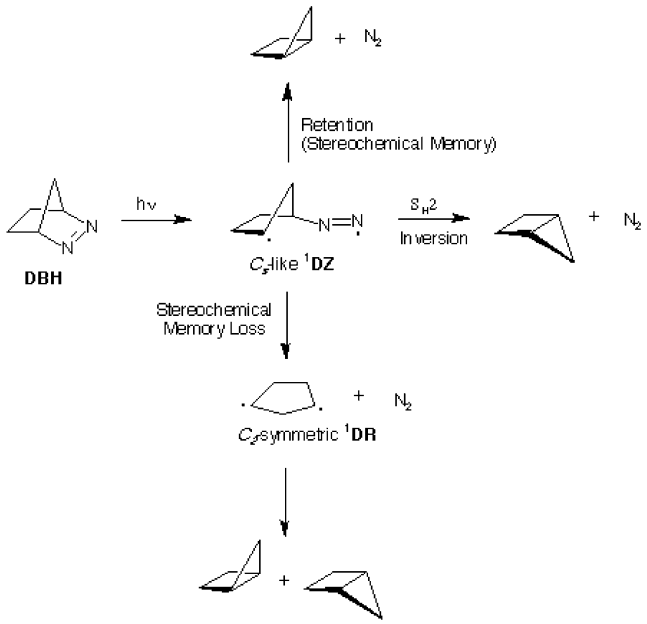


The conjecture that passage through the conical intersection generates, by relaxation along the ground-state energy surface, a diazenyl diradical **$^1$DZ** remains to be demonstrated. Furthermore, *a basic prerequisite to formulate a stereochemically defined mechanism for the production of housane consistent with the experimental facts is to establish computationally the nature and geometry of the initially formed (primary) conformation of the **$^1$DZ** intermediate*. For this reason, in the first part of this work, we present the results of unbiased (steepest descent) computations of the relaxation path by starting from n-$\pi$* **DBH**. We will show that the primary **$^1$DZ** conformation corresponds to a structure with an *exo-axial* $N_2$ group (Figure 2) and a $C_s$-*like* puckered cyclopentane-1,3-diyl ring (notice that in this mode, the carbon radical center at the C4 position is pyramidalized in the direction of the C−N bond). In the second part of this theoretical study we search, by starting from the *exo-axial* **$^1$DZ** conformation, for the pathways of housane formation described in Scheme 1.

The mechanistic analysis of the results discloses that all housane routes fall into a diradical region located in correspondence of a shallow energy well (0.0−4.0 kcal mol$^{-1}$) of the ground-state potential energy surface. Most importantly, it indicates that the dynamics prompted by the momentum gained through excited-state relaxation (i.e., in agreement with the Allred-Smith[4] and Carpenter[3] models), plays a key role in the stereochemistry of housane formation. Although the rigorous description of the photoinduced denitrogenation dynamics would require semiclassical or quantum-dynamics calculations, these methods are presently not practical for systems of the size of **DBH**, when high-quality energy surfaces are required. Thus, in the present paper, we extract qualitative information on the

(7) The $^1$n−$\pi$* **DBH** → **TS**α → **CI** path has now been fully recomputed at the same level of theory indicated in section 2.
(8) Adam, W.; Martí, V.; Sahin, C.; Trofimov, A. V. *J. Am. Chem. Soc.* **2000**, *122*, 5002−5003. Adam, W.; Diediring, M.; Trofimov, A. V. *Chem. Phys. Lett.* **2001**, *350*, 453−458.
(9) Adam, W.; Grüne, M.; Diediring, M.; Trofimov, A. V. *J. Am. Chem. Soc.* **2001**, *123*, 7109−7112.
(10) Adam, W.; Martí, V.; Sahin, C.; Trofimov, A. V. *Chem. Phys. Lett.* **2001**, *340*, 26−32.
(11) C2 axis passing through C1 and through the center of the C4−C5 bond of the 1,3-cyclopentadiyl structure (Sherrill, C. D.; Seidl, E. T.; Schaefer, H. F. III *J. Phys. Chem.* **1992**, *96*, 3712−3716).
(12) Adam, w.; García, H.; Martí, V.; Moorthy, J. N.; Peters, K.; Peters, E.-M. *J. Am. Chem. Soc.* **2000**, *122*, 3536−3537.

denitrogenation dynamics by inspection of accurate reaction paths[13] that are probed via classical trajectory computations. Our results allow to conclude the following: (a) Impulsive factors favor the $S_H2$ process; (b) when the impulsive motion is restrained, e.g., by strategically placed substituents or by increasing the medium viscosity, the production of inverted housane decreases; (c) restraint in the **$^1$DR**-ring motion from the "native" puckered *$C_s$-like* **$^1$DR** (or *$C_s$-like* **$^1$DZ**) conformation to the more persistent *$C_2$-symmetric* **$^1$DR** (or *$C_2$-like* **$^1$DZ**) conformation enhances the formation of retained housane; (d) while for the parent **DBH**, the diazenyl diradical corresponds to a shallow energy minimum, in bridgehead-substituted **DBH** derivatives this *exo-axial* **$^1$DZ** conformation only exist as a "snapshot" along the ground-state denitrogenation path.

## 2. Computational Methods

All molecular structures and reaction and relaxation coordinates presented in this paper have been obtained by unconstrained or constrained (see below) geometry optimization, with the complete active space self-consistent-field (CASSCF)[14] level of theory and a 6-31G* basis set.[15] The ground-state relaxation coordinate starting from the conical-intersection geometry, namely the *linear-axial* **CI** (Figure 1), has been computed by determining the initial relaxation direction and by following a previously reported procedure.[16] For all calculations, the active space chosen corresponds to 12 electrons in 10 orbitals. These comprise the $\sigma$ and $\sigma^*$ orbitals of the two **DBH** C−N bonds, the $\sigma$, $\sigma^*$, $\pi$, and $\pi^*$ orbitals of the N═N bond and the two nitrogen lone-pair ($n$) orbitals.

The accuracy of the results presented in this work suffers from an intrinsic limit due to the flatness of the potential energy surface of the **$^1$DZ** intermediate. Due to this flatness, different transition state structures could not be determined by unconstrained geometry optimization. In particular, all reaction paths for the **$^1$DZ** denitrogenation (dominated by the C1−N2 bond-breaking coordinate) and the change from the *$C_s$-like* to the *$C_2$-symmetric* conformation of the **$^1$DR** and **$^1$DZ** species (dominated by inversion of one radical center) have been investigated by constrained geometry optimization.[17] The reaction coordinate has then been computed by fixing the values of the constraint and by optimizing the energy along the remaining geometrical parameters.

To increase the accuracy of the computed energy barriers and transition structures, we have performed along the computed CASSCF reaction coordinate, single-point multireference-perturbation-theory computations by using the CASPT2 method[18] (for sake of simplicity *this CASPT2//CASSCF scheme will be indicated as CASPT2 level throughout the manuscript*). In Figure 3, we show the computed data for the denitrogenation path of the *exo-axial* **$^1$DZ** structure for the diazenyl diradical. It is evident that the position of the energy maximum and the magnitude of the reaction barrier changes significantly by passing from the CASSCF, which gives a 1.59 Å C1−N2 bond length and effectively a barrierless denitrogenation, to the CASPT2 level of theory. In fact, at the CASPT2 level, the C−N bond length becomes 1.55 Å and the dissociation barrier 3.6 kcal mol$^{-1}$. In principle, the most accurate reaction barrier and transition structure would be provided by CASPT2 geometry optimization. Regrettably, this type of calculation

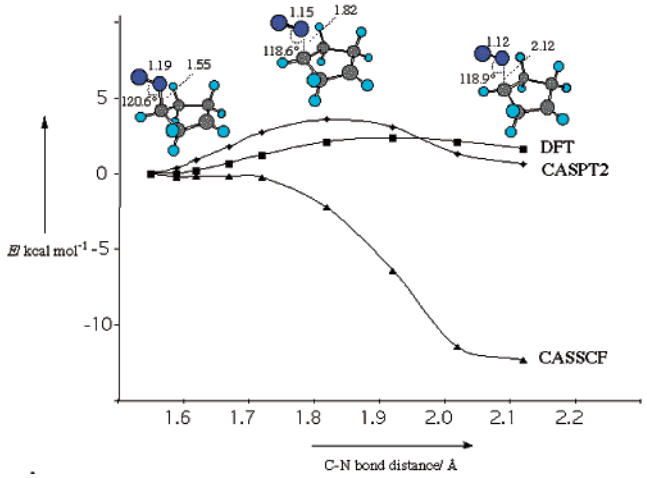


***Figure 3.*** CASSCF (full triangles), CASPT2 (full diamonds), and triplet DFT (full squares) energy profiles for the denitrogenation of the diazenyl diradical *exo-axial* **$^1$DZ**. The structures document the molecular changes along the reaction coordinate. The geometrical parameters for the $N_2$ departure are given in Å and degrees.

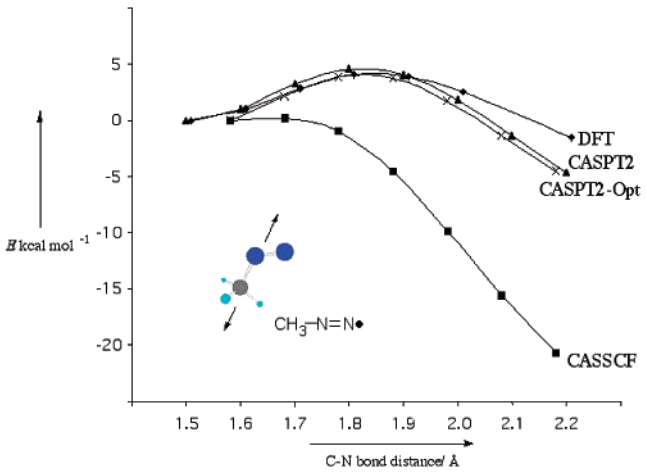


***Figure 4.*** CASSCF (full triangles), CASPT2-Opt (full diamonds), CASPT2 (crosses) and triplet DFT (full squares) energy profiles for the denitrogenation of the methyl diazenyl diradical as model system. Comparison of the CASPT2 and CASPT2-Opt energy indicates that the CASPT2//CASSCF scheme used in this paper provides a good approximation for evaluating reaction barriers.

is still not practical for systems as large as **DBH**. To validate the energy profile computed in Figure 3 (obtained by single-point CASPT2 computations on a reaction coordinate computed at the CASSCF level), we have evaluated the CASPT2 reaction coordinate (by C−N constrained optimization and by using numerical gradients—CASPT2-Opt level) for the C−N bond cleavage of the methyl diazenyl radical as model system (Figure 4). This computation demonstrates that the transition structures and the CASPT2 energy barriers computed with the CASSCF and the CASPT2 reaction coordinates are similar. For this reason, in the following section, we will exclusively present energy barriers and stationary points (minima and transition structures) determined by using the CASPT2//CASSCF strategy defined above. As reported elsewhere,[19] this strategy predicts energy barriers of 7.6 and 11.4 kcal mol$^{-1}$ for the α cleavage of the C−N bond in singlet-excited pyrazoline and diazabicyclo[2.2.2]octene (azoalkanes closely related to **DBH**). This compares well with the experimental values of 6−9 kcal mol$^{-1}$ for pyrazoline and 8.6−10.2 kcal mol$^{-1}$ for diazabicyclo-[2.2.2]octene derivatives. The pathway for the conformational change

(13) Garavelli, M.; Bernardi, F.; Olivucci, M.; Vreven, T.; Klein, S.; Celani, P.; Robb, M. A. *Faraday Discussion* **1998**, *110*, 51−70.
(14) Roos, B. O. *Complete Active Space Self-Consistent Field Method and its Applications in Electronic Structure Calculations*; Wiley: New York, 1987; Vol. 69.
(15) Hehre, W. J.; Radom, L.; Schleyer, P. V. R.; Pople, J. A. *Ab Initio Molecular Orbital Theory*; Wiley: New York, 1986.
(16) Celani, P.; Robb, M. A.; Garavelli, M.; Bernardi, F.; Olivucci, M. *Chem. Phys. Lett.* **1995**, *243*, 1−8.
(17) The constraint has been defined as the C−N bond length and the C−H inversion angle.
(18) Andersson, K.; Malmqvist, P.-A.; Ross, B. O. *J. Chem. Phys.* **1992**, *96*, 1218−1226.
(19) Nau, W. M.; Greiner, G.; Wall, J.; Rau, H.; Olivucci, M.; Robb, M. A. *Angew. Chem., Int. Ed. Engl.* **1998**, *37*, 98−101.

***Scheme 2.*** "Roadmap" of Mechanistic Pathways (path a-e) for the Competitive Denitrogenations of the *Exo-axial* ($C_s$*-like*) Singlet Diazenyl Diradical ($^1$DZ) to the Inverted and Retained Housanes in the Photolysis of Azoalkane DBH. the Values (in kcal mol$^{-1}$) above the Arrows (italics) Stand for Activation Barriers and the Ones below the Structures (bold-face) for Reaction Enthalpies

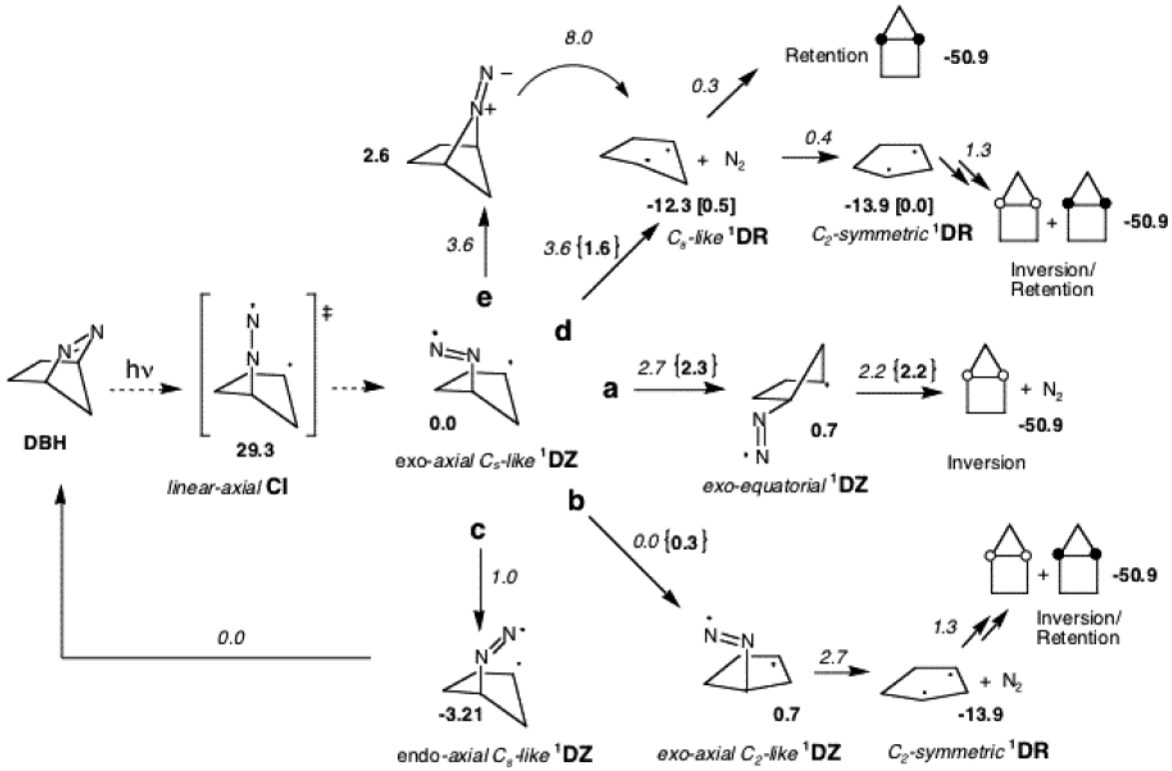


of the structure for the $^1$**DZ** species from the $N_2$-*exo* to the $N_2$-*endo* conformation along the C1−N2 internal rotation has also been investigated at the CASPT2 level. As described above for the pathways dominated by the C1−N2 bond breaking, the coordinate for the *exo*-to-*endo* change has been computed by fixing the values of the torsion about the C1−N2 bond and by optimizing the energy along the remaining geometrical parameters. Furthermore, in this case, the value of the C−N bond length has also been kept fixed at its optimal CASPT2 value (1.55 Å) to avoid C−N bond breaking during the optimization.

To describe the $S_H2$ pathway connecting the *exo-axial* $^1$**DZ** to the *exo-equatorial* $^1$**DZ** structure we have computed a series of intermediate geometries via interpolation of the axial-to-equatorial metastable conformer discuss below with the *exo-axial* $^1$**DZ** and *exo-equatorial* $^1$**DZ**. For each structure the C−N bond length has been optimized at the CASPT2 level as described above.

The ZPE correction to the barriers of paths **a** (*exo-axial* $^1$**DZ** to *exo-equatorial* $^1$**DZ** ring-inversion), path **b** (*exo-axial Cs-like* $^1$**DZ** to *exo-axial* $C_2$*-like* $^1$**DZ**) and path **d** (nitrogen extrusion from the *exo-axial* $^1$**DZ**) of Scheme 2 have been evaluated at the singlet UB3LYP level of theory (see also discussion below). The frequency calculations have been performed using UB3LYP optimized structures. These are obtained via constrained geometry optimization (i.e., fixing the C−N distance at the CASPT2 optimum C−N bond distance—the constrain is required since the UB3LYP level yields an unbound $^1$**DZ** C−N bond).

For the only case of the change from the $C_s$*-like* to the $C_2$*-symmetric* conformation of the $^1$**DR** species we have been able to perform a fully unconstrained geometry optimization at the CASPT2 level (again by using numerical gradients) of the equilibrium structure of the two $^1$**DR** conformers. These results will be discussed in Section 3.3.

The stereochemistry of the photochemical **DBH** denitrogenation has also been experimentally determined as a function of the substitution pattern[8] and, recently, by using different bridgehead substituents.[10] Thus, we also computed the sensitivity of the $^1$**DZ** denitrogenation as a function of methyl, ethyl and phenyl bridgehead substituents. Due to the increase in the size of the system (especially in the case of the phenyl substituent), we have investigated the denitrogenation process of $^1$**DZ** by means of density functional theory (DFT) at the singlet UB3LYP[20]/6-31G* level. To validate this strategy, to be employed for the most computationally demanding reaction path, in Figure 4 we compare energy barriers and transition-state position of the methyl diazenyl radical model with the corresponding DFT path. It is apparent that the DFT energy profile is quite close to the "correct" CASPT2 energy profile. For this reason, and similar to the strategy adopted for the evaluation of the CASPT2 energy profile, we have computed the DFT reaction paths by single-point DFT calculations on the CASSCF-optimized structure. (Notice that in the diradical region of the ground-state energy surface both singlet and triplet UB3LYP/6-31G* reproduce the CASPT2 level energy profiles better then CASSCF). For the same reason, singlet DFT is also used for ZPE (i.e., frequency computations). However, as mentioned above, in this case we employ the DFT equilibrium structure. As shown in Figure 3 for $^1$**DZ** denitrogenation, the computation produces again a curve close to the CASPT2 result. In conclusion, the following strategy has been used to assess the substituent effects on the denitrogenation of the $^1$**DZ** intermediate. The substituents have been added to the CASSCF optimized reaction-coordinate structures by simply replacing the bridgehead hydrogen with the substituent. For each reaction-coordinate structure we have carried out constrained geometry optimizations at the DFT level by only relaxing the structure of the bridgehead substituent and the bond lengths and planar angles of the **DBH** hydrocarbon skeleton (the C−N bond length and all the dihedral angles have been kept fixed at the corresponding CASSCF values).

As detailed in Subsection 3.4, due to the fact that the singlet DFT overestimate the stability of closed-shell intermediates with respect to diradical structures, the triplet DFT level is used for classical trajectory computations. These are used to probe the ground state relaxation dynamics occurring immediately after the excited state decay. Accordingly two different trajectories are computed starting near the linear-

axial CI. The first trajectory is released without initial velocity. The second trajectory is released with a velocity proportional to the energy difference between TSα and linear-axial CI so that to mimic the effect of the excited-state relaxation. Such initial velocity is specified in terms of mass weighted Cartesian components. The direction of the velocity vector has been assumed to be identical to that of the ground-state force.

All CASSCF and DFT computations have been carried out with the GAUSSIAN98 series of programs.[21a] The CASPT2 computations have been conducted with the MOLCAS-4 package.[22] DFT trajectory computations have been carried out with GAUSSIAN03.[21b]

## 3. Results and Discussion

The results are summarized in Scheme 2 (values in italic indicate reaction barriers and values in bold indicate relative stabilities). The excited-state branch of the reaction pathway (dashed arrows) leads to the $C_s$-like *exo-axial* **$^1$DZ** intermediate exclusively. This intermediate may evolve along five different ground-state pathways, all located within 0.0−4.0 kcal mol$^{-1}$. Three pathways (paths **a**, **b**, and **c**) are characterized by an initial conformational change, whereas the remaining pathways are characterized by initial C−N bond-breaking (path **d**) and C−N bond-making (path **e**) events. From the stereochemical point of view, path **a** is the only trajectory that produces inverted housane. The paths **e** and **d** lead mainly to retained housane, and path **b** to a 1:1 mixture of inverted and retained housanes. In the following subsections, we discuss the main features of these paths and their role in the stereochemistry of the **DBH** denitrogenation.

**3.1 Excited-State Relaxation.** In this subsection, we document the nature of the reaction coordinate that goes from the equilibrium structure of the $^1$n-$\pi$*-excited **DBH** molecule to the primary ground-state **$^1$DZ** conformation (see dashed arrows in Scheme 2). In a previous report,[6] the $^1$n-$\pi$* branch of the reaction coordinate, which includes the α-cleavage event, had been documented at a level of theory that did not allow for a quantitative evaluation of the reaction energy profile. This part has now been recomputed at the CASPT2 level.

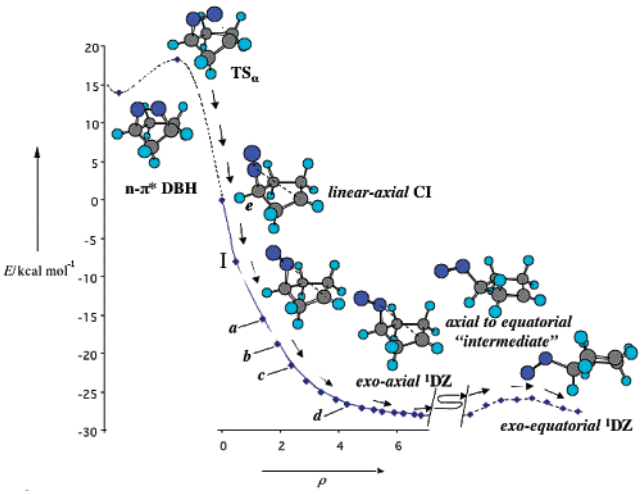


***Figure 5.*** CASPT2 energy profile along the photochemical α-cleavage pathway of $^1$n-$\pi$* **DBH**. The excited-state branch of the reaction is described by the $^1$n-$\pi$* **DBH** equilibrium structure, α-cleavage transition structure **TS**$_\alpha$, and the conical-intersection *linear-axial* **CI** geometry. The ground-state branch is documented by the relaxation pathway (the steepest descent path), which starts at the *linear-axial* **CI** structure and ends at the primary *exo-axial* **$^1$DZ** intermediate. Also the secondary generation of the *exo-equatorial* conformation for the *exo-axial* **$^1$DZ** structure is documented by including the energies of the axial-to-equatorial transition structure and of the equilibrium structure of the *exo-equatorial* **$^1$DZ** intermediate. The structures document the molecular changes along the reaction coordinate. Point **I** corresponds to the point where classical trajectory are released (see Subsection 3.4).

In Figure 5 we show that in order to achieve α cleavage, the n-$\pi$*-excited **DBH** molecule must overcome a barrier of 5.7 kcal mol$^{-1}$ at the **TS**$_\alpha$ point. As shown for other azoalkanes such as pyrazoline and diazabicyclo[2.2.2]octene,[19] this barrier determines the lifetime of the excited **DBH** as it drives the system toward the conical-intersection funnel, where decay of excited **DBH** to the ground state **$^1$DZ** occurs. As previously reported,[6] the electronic structure of the reacting species changes along the energy path. At the **TS**$_\alpha$ point, a $\sigma,\pi$ singlet diazenyl diradical ($\sigma,\pi$-**DZ**) is formed initially, which expectedly denitrogenates reluctantly, because the high-energy n,$\pi$*-excited $N_2$ molecule would result, as already predicted qualitatively on the basis of a Salem diagram.[23] However, after the **TS**$_\alpha$ transition state, the molecule evolves toward the conical intersection located ca. 20 kcal mol$^{-1}$ lower in energy, where the $\sigma,\pi$ and $\sigma,\sigma$ states of the diazenyl diradical cross.[6] Thus, decay to the ground state through the conical intersection leads to the $\sigma,\sigma$ singlet diazenyl diradical ($\sigma,\sigma$-**DZ**).

It is essential for the present work to provide a quantitative description of the formation of the ground-state primary photoproduct, namely the *exo-axial* **$^1$DZ** species, by determining the evolution of the $^1$n-$\pi$* **DBH** reactant through **TS**$_\alpha$ and the following *linear-axial* **CI**. Thus in Figure 5, we show that the steepest-descent path computed starting from the conical-intersection, leads to an *exo-axial* **$^1$DZ** conformation, located 48.7 kcal mol$^{-1}$ below the **TS**$_\alpha$ point. For this structure, the cyclopentane-1,3-diyl ring shows a $C_s$-*like* conformation due

(20) Lee, C.; Yang, W.; Parr, R. G. *Phys. Rev. B* **1988**, *37*, 785. Becke, A. D. *Phys. Rev. A* **1988**, *38*, 3098. Becke, A. D. *J. Chem. Phys.* **1993**, *98*, 5648. Stephens, P. J.; Devlin, F. J.; Chabalowski, C. F.; Frish, M. J. *J. Phys. Chem.* **1994**, *98*, 11 623−11 627.

(21) (a) Frisch, M. J.; Trucks, G. W.; Schlegel, H. B.; Scuseria, G. E.; Robb, M. A.; Cheeseman, J. R.; Zakrzewski, V. G.; J. A. Montgomery, Jr.; Stratmann, R. E.; Burant, J. C.; Dapprich, S.; Millam, J. M.; Daniels, A. D.; Kudin, K. N.; Strain, M. C.; Farkas, O.; Tomasi, J.; Barone, V.; Cossi, M.; Cammi, R.; Mennucci, B.; Pomelli, C.; Adamo, C.; Clifford, S.; Ochterski, J.; Petersson, G. A.; Ayala, P. Y.; Cui, Q.; Morokuma, K.; Malick, D. K.; Rabuck, A. D.; Raghavachari, K.; Foresman, J. B.; Cioslowski, J.; Ortiz, J. V.; Baboul, A. G.; Stefanov, B. B.; Liu, G.; Liashenko, A.; Piskorz, P.; Komaromi, I.; Gomperts, R.; Martin, R. L.; Fox, D. J.; Keith, T.; Al-Laham, M. A.; Peng, C. Y.; Nanayakkara, A.; Gonzalez, C.; Challacombe, M.; Gill, P. M. W.; Johnson, B.; Chen, W.; Wong, M. W.; Andres, J. L.; Gonzalez, C.; Head-Gordon, M.; Replogle, E. S.; Pople., J. A. In; *Guassian98*, Revision A.7 ed.; Gaussian, Inc.: Pittsburgh, PA, 1998. (b) Frisch, M. J.; Trucks, G. W.; Schlegel, H. B.; Scuseris, G. E.; Robb, M. A.; Cheeseman, J. R.; Montgomery, J. J. A.; Vreven, T.; Kudin, K. N.; Burant, J. C.; Millam, J. M.; Iyengar, S. S.; Tomasi, J.; Barone, V.; Mennucci, B.; Cossi, M.; Scalmani, G.; Rega, N.; Petersson, G. A.; Nakatsuji, H.; Hada, M.; Ehara, M.; Toyota, K.; Fukuda, R.; Hasegawa, J.; Ishida, M.; Nakajima, T.; Yonda, Y.; Kitao, O.; Nakai, H.; Klene, M.; Li, X.; Knox, J. E.; Hratchian, H. P.; Cross, J. B.; Adamo, C.; Jaramillo, J.; Gomperts, R.; Stratmann, R. E.; Yazyev, O.; Austin, A. J.; Cammi, R.; Pomelli, C.; Ochterski, J. W.; Ayala, P. Y.; Morokuma, K.; Voth, G. A.; Salvador, P.; Dannenberg, J. J.; Zakrzewski, V. G.; Dapprich, S.; Daniels, A. D.; Strain, M. C.; Farkas, O.; Malick, D. K.; Rabuck, A. D.; Raghavachari, K.; Foresman, J. B.; Ortiz, J. V.; Cui, Q.; Baboul, A. G.; Clifford, S.; Cioslowski, J.; Stefanov, B. B.; Liu, G.; Liashenko, A.; Piskorz, P.; Komaromi, I.; Martin, R. L.; Fox, D. J.; Keith, T.; Al-Laham, M. A.; Peng, C. Y.; Nanayakkara, A.; Challacombe, M.; Gill, P. M. W.; Johnson, B.; Chen, W.; Wong, M. W.; Gonzalez, C.; Pople, J. A. Revision B.04 Ed., Gaussian, Inc., Pittsburgh PA, 2003.

(22) Andersson, K.; Blomberg, M. R. A.; Fülscher, M. P.; Karlström, G.; Lundh, R.; Malmqvist, P.-A.; Neogrády, P.; Olsen, J.; Roos, B. O.; Sadlej, A. J.; Schütz, M.; Seijo, L.; Serrano-Andrés, L.; Siegbahn, P. E. M.; Widmark, P.-O. In; Version 4 ed.; University of Lund: Lund, Sweden, 1997.

(23) Adam, W.; Oppenländer, T.; Zang, G. J. *J. Org. Chem.* **1985**, *50*, 3303−3312. Adam, W.; Denninger, U.; Finzel, R.; Kita, F.; Platsch, H.; Walter, H.; Zang, G. *J. Am. Chem. Soc.* **1992**, *114*, 5027−5035.

to the fact that the C−H bond at the radical center still reflects the original pyramidalization in **DBH**. The data in Figure 5 also suggest that the initially formed *$C_s$-like exo-axial* $^1$**DZ** intermediate will dissipate a large amount (ca. 50 kcal mol$^{-1}$) of excess kinetic energy during the following ground state evolution. It is, thus, of primary importance to determine the ground-state pathway that may be impulsively populated after excited-state relaxation. For this purpose, we have carried out an internal-coordinate analysis of the computed relaxation path (i.e. by compare structures **TS**$_\alpha$, *linear-axial* **CI** and *exo-axial* $^1$**DZ**) that leads to the following conclusions:

(i) The **TS**$_\alpha$ → *exo-axial* $^1$**DZ** evolution is primarily dominated by the C1−N2−N3 (see structure **TS**$_\alpha$ in Figure 1 for the atom numbering) bending coordinate, which undergoes more than a 120° *inversion* from the $N_2$-*endo* (**TS**$_\alpha$) to the $N_2$-*exo* (*exo-axial* $^1$**DZ**) conformation.

(ii) The C1−N2 elongation also contributes to the relaxation because the C−N bond length increases by ca. 0.04 Å along the **TS**$_\alpha$ → *exo-axial* $^1$**DZ** path. Notice that, as discussed above, reevaluation of the C−N equilibrium bond lengths and barriers for the *exo-axial* $^1$**DZ** structure (see Figure 3) shows that at the CASPT2 level of theory the C−N bond becomes shorter (from 1.59 Å to 1.55 Å) and stabilized (C−N breaking barrier increases from <1 kcal mol$^{-1}$ to 3.6 kcal mol$^{-1}$. This barrier becomes 1.6 kcal mol$^{-1}$ after ZPE correction. See value in curly brackets in Scheme 2) with respect to the CASSCF level used to compute the relaxation coordinate. This change is not expected for the fully intact C−N bonds in the **TS**$_\alpha$ and *linear-axial* **CI** species.

(iii) A limited and late ring planarization and a more limited planarization of the incipient radical center at the C4 position occur during the excited-state (**TS**$_\alpha$ → *linear-axial* **CI**) relaxation. The ring planarization is documented by the decrease in the C4−C7−C1−C6, C5−C4−C7−C1 and C6−C5−C4−C7 dihedral angles. For the radical center, the planarization process is documented by a decrease of the formal H4−C7−C5−C4 dihedral angle from a 17 to 10 degrees (H4 indicates the H bounded to C4).

(iv) The relaxation coordinate has no components along the *torsion* that describes the *exo*-to-*endo* conformational change by internal rotation about the C1−N2 bond.

(v) The C4- - -N2 distance decreases monotonically along the initial part (i.e., from linear-axial **CI** (C4−N2 = 2.94 Å) to structure **c** (C4−N2 = 2.78 Å)) of the relaxation path and is therefore coupled with the decreasing C1−N2−N3 bending angle.

**3.2 $S_H2$ Pathway.** Above, we have seen that the C1−N2−N3 bending motion dominates the evolution of the *exo-axial* $^1$**DZ** species from **TS**$_\alpha$. In a structure where the N−N is bounded to the ring, the acquired momentum may induce the axial-to-equatorial ring inversion (path **a** in Scheme 2) by impulsively pushing the C1 site across the ring plane. This is driven by the fact that the C−N−N mode becomes stiff for small values of the angle. To support the idea that the acquired momentum will contribute to the axial-to-equatorial ring inversion we have plotted the gradient vector for four selected structures belonging to the terminal part of the computed relaxation coordinate. These structures and the related normalized gradient vectors are given in Scheme 3. The labels **a**, **b**, **c**, and **d** in Figure 5 indicate the position of the associated structure along the relaxation coordinate. It is apparent from inspection of structure **a**−**c** that in the initial part of the relaxation ring inversion motion is not coupled to the C−N−N bending. In fact, as pointed out in point (v) above, in the initial part of the relaxation path (from linear-axial **CI** to **c**) the bending seems coupled with the C4- - -N2 distance decrease. In contrast, it is apparent from inspection of structure **d** that in the terminal part of the relaxation path ring motion is coupled to the C−N−N bending (leading to C4- - -N2 distance increase) suggesting that the relaxation coordinate changes character (i.e., is bent) in its terminal part (also consider that at *exo-axial* $^1$**DZ** the C4−N2 distance is further expanded to 3.0 Å).

***Scheme 3.*** Four Sequential "snapshot" (structure a, b, c, d in Figure 5) along the Excited-state Relaxation Path Showing the Component of the Gradient along the Path Leading to the *Exo-axial* (*$C_s$-like*) Singlet Diazenyl Diradical ($^1$DZ)

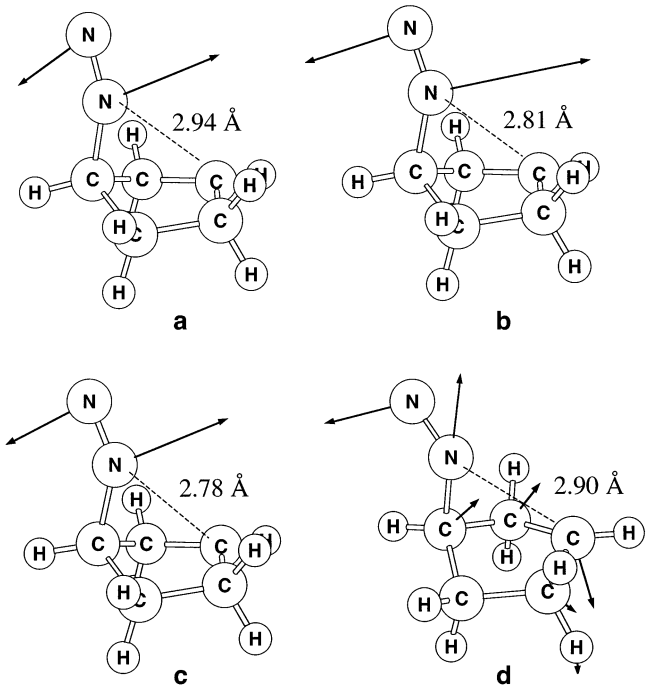


To evaluate the accessibility of path **a**, we performed a detailed mapping of the ring inversion pathway and probe its impulsive population via classical trajectory computations.

In Figure 5, we show that the computed axial-to-equatorial ring inversion path reveals the existence of a very flat region where lies an axial-to-equatorial intermediate conformer displaying a flat cyclopentadiyl ring. The potential energy region centered on this intermediate is extremely flat and therefore this may be seen either as a highly unstable intermediate or a flat transition structure located 2.7 kcal mol$^{-1}$ above *exo-axial* $^1$**DZ**. This barrier becomes 2.3 kcal mol$^{-1}$ after ZPE correction. (See value in curly brackets in Scheme 2). Therefore, ca. one twentieth of the initial momentum is enough to push the initial *exo-axial* $^1$**DZ** intermediate through the barrier to yield the *exo-equatorial* conformer. In principle, this *exo-equatorial* $^1$**DZ** intermediate is a suitable starting point for the production of the inverted housane. The energy profile given in Figure 6 demonstrates that there is a barrier to denitrogenation of 2.2 kcal mol$^{-1}$. This barrier remains 2.2 kcal mol$^{-1}$ after ZPE correction. Analysis of the corresponding reaction coordinate shows the following: (a) The incipient cylopentane-1,3-diyl radical conformation does not persist, but immediately yields

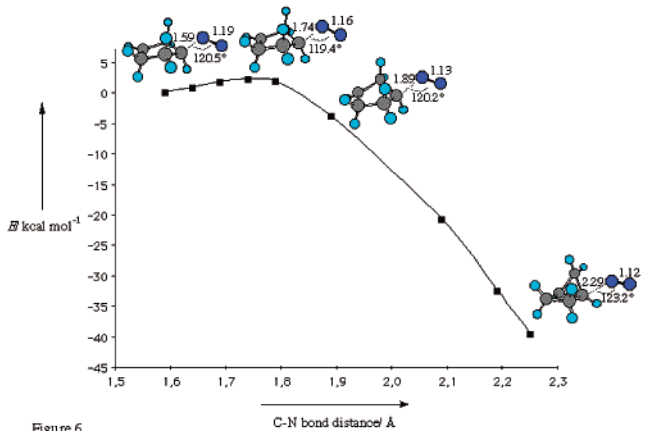


***Figure 6.*** CASPT2 energy profile along the denitrogenation path of the *exo-equatorial* **$^1$DZ** intermediate. The structures document the molecular changes along the reaction coordinate. The geometrical parameters for the $N_2$ departure are given in Å and degrees.

the inverted housane; (b) the reaction coordinate for $N_2$ departure does not seem to involve any significant contribution of the N2−N3 stretching and C1−N2−N3 bending mode that would result in vibrational and rotational excitation of the departing $N_2$ fragment.

To provide information on the impulsive dynamics following the relaxation from *linear-axial* **CI**, in Subsection 3.4 we present and analyze the result of two different DFT classical trajectory computations. It is shown that, within the approximation related to the use of a DFT force field, both trajectories yield impulsively (within 200 fs) either an inverted cyclopentadiyl diradical (that, in turn, produces inverted housane via radical coupling) or an *exo-equatorial* **$^1$DZ** intermediate (that produces inverted housane via the classic $S_H2$ mechanism). No population of other competitive paths is observed.

On the basis of these results, we conclude that an impulsively populated axial-to-equatorial conformational change results in a concerted production of inverted housane. Thus, we validate the $S_H2$ mechanism (see Scheme 1) at the level of theory employed in this computational work, with the *exo-equatorial* **$^1$DZ** *structure* as its short-lived precursor.

**3.3 *exo-axial* $^1$DZ Denitrogenation, Conformational Change and "Cold" Processes.** As mentioned in Subsection 3.1, the analysis of the relaxation coordinate indicates that a part of the initial excess energy populates the C1−N2 elongation mode. This suggests that a second reaction pathway could be impulsively populated, namely the denitrogenation of the initially generated *exo-axial* **$^1$DZ** conformation (path **d** in Scheme 2). The computed energy barrier along this mode is 3.6 kcal mol$^{-1}$ (1.6 kcal mol$^{-1}$ after ZPE correction). Again, less than one twentieth of the initial excess energy will be required to populate this pathway for the production of a puckered *$C_s$-like* **$^1$DR** intermediate (Figure 7). This diradical may then either ring-close to generate retained housane (despite several attempts, a concerted pathway from the *exo-axial* **$^1$DZ** structure to the retained housane could not be located) or undergo a conformational change to the lower-energy *$C_2$-symmetric* conformation. This symmetrical conformation leads to a 1:1 mixture of inverted and retained housanes. Notice that the puckered *$C_s$-like* **$^1$DR** species (path **d**) may nearly competitively afford the retained housane (0.3 kcal mol$^{-1}$ barrier) and the *$C_2$-symmetric* **$^1$DR** (0.4 kcal mol$^{-1}$ barrier). Thus, formation of the *$C_s$-like* **$^1$DR** intermediate through path **d** could be the prevalent route to the retained housane and thereby be responsible for a possible memory effect (Scheme 1).

It is important to stress that the puckered *$C_s$-like* **$^1$DR** intermediate seems to be substantiated by dynamic electron correlation. Indeed, such a transient lies ca. 6.2 kcal mol$^{-1}$ higher in energy than the *$C_2$-symmetric* **$^1$DR** species at the uncorrelated CASSCF level of theory (the CASSCF frequency computations for the *$C_s$-like* **$^1$DR** intermediate reveal two imaginary frequencies for the pyramidalizing inversion motion at the C1 and C4 radical centers). Nevertheless, at the correlated CASPT2 level, the *$C_s$-like* **$^1$DR** is only 1.6 kcal mol$^{-1}$ higher than the *$C_2$-symmetric* **$^1$DR** diradical. As a result the energy profile for the *$C_s$-like* → *$C_2$-symmetric* conformational change shows, as mentioned above, a small (0.4 kcal mol$^{-1}$) barrier and suggests that a puckered **$^1$DR** diradical may correspond to a topologically defined conformer of finite existence. This conclusion has been further investigated by performing the first CASPT2 geometry optimization of the *$C_s$-like* and *$C_2$-symmetric* **$^1$DR** conformations based on a numerical gradient procedure. The computations successfully locate two equilibrium structures which differ by only 0.5 kcal mol$^{-1}$ (see values in square brackets in Scheme 2) and whose relevant geometrical parameters are given in Figure 7 (see values in square brackets). For this reason, in the following we treat the *$C_s$-like* **$^1$DR** species as a distinct mechanistic entity.

According to the analysis in Subsection 3.1, excited-state relaxation may also create some momentum along the ring

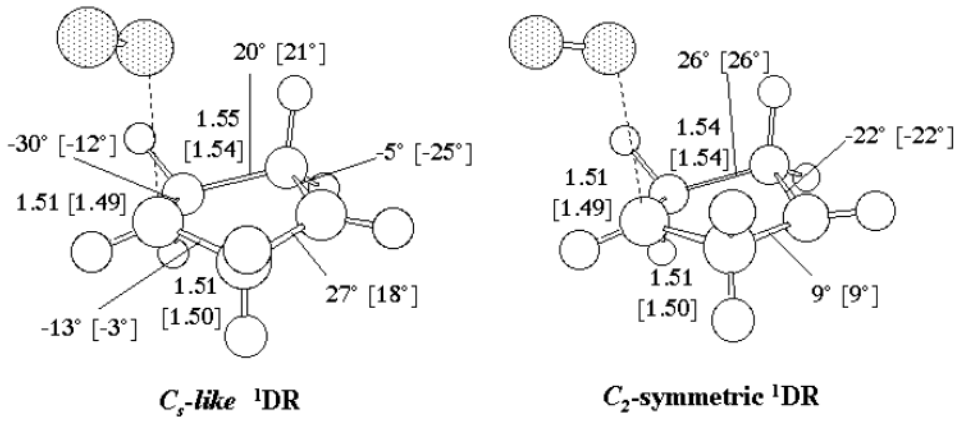


***Figure 7.*** Computed geometries for the *$C_s$-like* and *$C_2$-symmetric* singlet cyclopentane-1,3-diyl diradicals (**$^1$DR**).

planarization and C4 inversion modes if the terminal part of the path gets populated. This suggests an impulsive *$C_s$-like* → *$C_2$-like* conformational change of the *exo-axial* $^1$**DZ** structure (path **b** in Scheme 2). Again, this implies impulsive production of a *$C_2$*-like *exo-axial* $^1$**DZ** intermediate as a precursor of the *$C_2$-symmetric* $^1$**DR** species and ultimately a 1:1 mixture of inverted and retained housane should result. Population of path **b** could be favored relative to path **d** by the low barrier (<1 kcal mol$^{-1}$) for the production of the *$C_2$-like exo-axial* $^1$**DZ** species. Furthermore, along path **b**, the total barrier for the generation of the *$C_2$-symmetric* $^1$**DR** intermediate is 0.9 kcal mol$^{-1}$ (considering the same ZPE correction computed for path **d**) lower than the barrier along path **d**. Consequently, our computations reveal path **b** as the major route to a 1:1 mixture of inverted and retained housanes (Scheme 1).

Possible impulsive population of the cyclization mode corresponding to path **e** (which also requires further puckering of the original cyclopentane-1,3-diyl ring) is suggested by the fact that the C4- - -N2 distance decreases along the initial part of the relaxation path of Figure 5 (see discussion in section 3.2). However, under the conditions of complete equilibration, path **e** will not contribute significantly (at least for the parent **DBH**) to the denitrogenation and housane formation because the total barrier to achieve the puckered *$C_s$-like* $^1$**DR** species through this pathway should be as high as 10.6 kcal mol$^{-1}$.

In principle, the paths **a**, **b**, and **d** could also compete with paths **c** (see Scheme 2); however, our relaxation-path analysis indicates that the modes which characterize these alternative pathways will not be impulsively populated. In fact, the *exo*→*endo* torsional coordinate of path **c** (the torsion about the C1−N2 bond) does not contribute to the excited-state relaxation. Thus, paths **c** is accessed by "cold" (dynamically disfavored) modes and will only be populated if the lifetime of the *exo-axial* $^1$**DZ** structure is long enough to allow thermal equilibration (internal vibrational energy redistribution). In agreement with previous results,[6] the *exo-axial*-to-*endo-axial* conformational change of the $^1$**DZ** diradical along the path **c** appears to be a facile process, controlled by a low (ca. 1 kcal mol$^{-1}$) torsional barrier in direction of the methylene bridge. As soon as the *$C_s$-like endo-axial* $^1$**DZ** conformation is produced, a barrierless ring closure regenerates **DBH**. This indicates that our computed *$C_s$-like endo-axial* $^1$**DZ** conformation corresponds to a labile structure, prone to recyclize to **DBH** rather than denitrogenate to the $^1$**DR** diradical.

**3.4 Probing the Ground-State Relaxation Path using Classical Trajectories.** CASPT2 and even CASSCF classical trajectories cannot be presently computed for a system of the size of DBH. For this reason, we have checked if DFT could provide a realistic force field for probing the impulsive (i.e., short time scale) dynamics behavior of DBH following excited-state decay. Thus in Figure 8 we compare the CASPT2 energy profile of Figure 5 with the corresponding energy profiles of the paths computed at the singlet and triplet DFT levels. We also compare the stationary points along the inversion path with the corresponding singlet and triplet DFT stationary points. In all cases, structure I of Figure 5 (i.e., the first point along the ground-state relaxation path) is taken as the initial structure of the energy profile (i.e., this point is not re-optimized at the DFT levels). Also the relaxed *exo-axial* $^1$**DZ** intermediate is taken as the reference point for the description of the energetics.

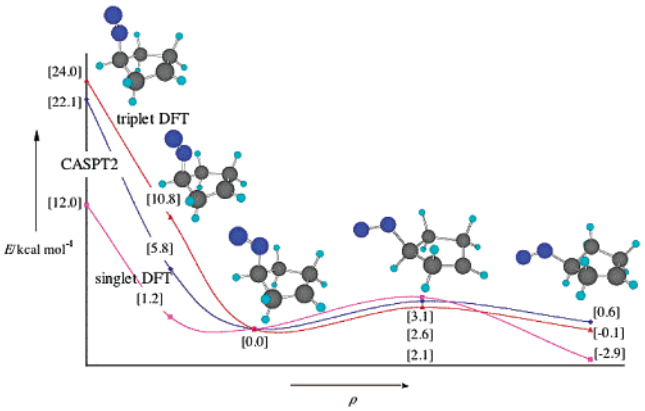


***Figure 8.*** Comparison of the CASPT2 energy profile of Figure 5 with the corresponding energy profiles of the paths computed at the singlet and triplet DFT levels. The structures document the molecular changes along the reaction coordinate.

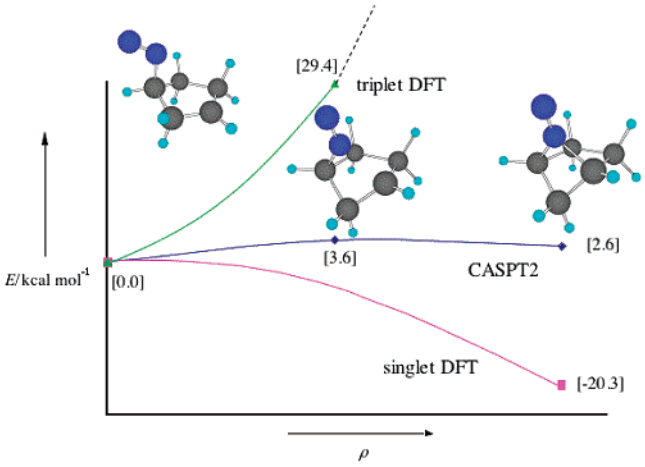


***Figure 9.*** Triplet DFT (full triangles), CASPT2 (full diamonds), and singlet DFT (full squares) energy profiles for path **e** (see Scheme 2). The structures document the molecular changes along the reaction coordinate.

It is apparent from inspection of Figure 8 that although singlet DFT seriously underestimates the slope of the energy profile driving the initial relaxation, triplet DFT has an energy profile much closer to the "exact" CASPT2 profile (one has a max difference of 5 kcal mol$^{-1}$ in the central region of the slope). On the other hand, as mentioned earlier, along the axial-to-equatorial inversion path both levels provide a qualitatively acceptable description with the triplet level overestimating the stability of the *exo-equatorial* $^1$**DZ** intermediate of 3.5 kcal mol$^{-1}$.

In Figure 9, we further probe the singlet and triplet DFT energetics with respect to path **e**. This test is necessary because the relaxation path analysis of Section 3.2 indicates a large coupling between the C1−N2−N1 bending and C4- - -N2 distance along the initial part of the relaxation path. Momentum acquired in this direction will displace the system toward the bicyclic intermediate reported in Scheme 2 prompting population of path **e** (see also Subsection 3.3). It is clear from Figure 9 that the singlet DFT overestimates the stability of the bicyclic structure of ca. 20 kcal mol$^{-1}$, and it is therefore not acceptable. Indeed, along this displacement the *exo-axial* $^1$**DZ** intermediate has an extremely flat negative curvature and it is not a stable intermediate. In contrast, the same diradical is highly stable at the triplet DFT level. On the other hand, at the triplet level the

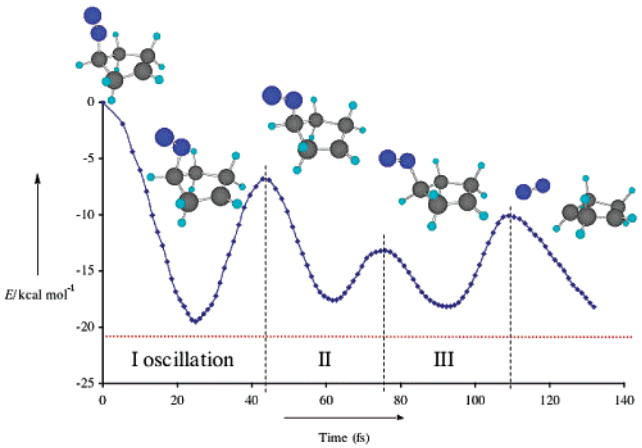


***Figure 10.*** Triplet DFT energy profile along the trajectory computations started at structure I in Figure 5 (i.e., the first point along the ground-state relazation path) without initial kinetic energy. The structures document the molecular changes along the simulation.

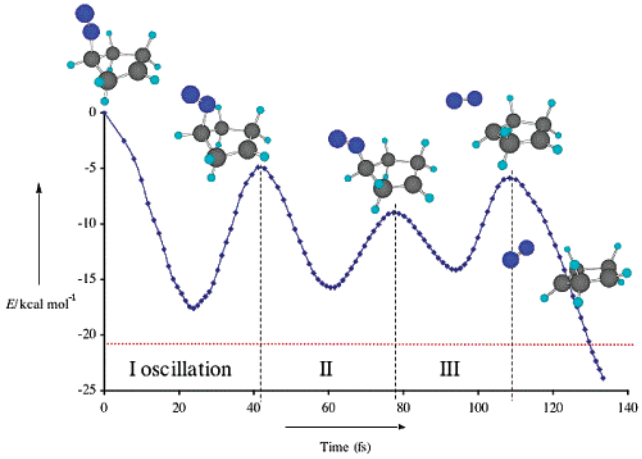


***Figure 11.*** Triplet DFT energy profile along the trajectory computations started at structure I in Figure 5 (i.e., the first point along the ground-state relazation path) with a nonzero initial kinetic. The structures document the molecular changes along the simulation.

displacement toward the bicyclic structure leads to a rapid energy increase due to the repulsion of the two triplet spin-coupled radical centers. It is thus concluded that neither singlet nor triplet DFT describes path **e** correctly. On the other hand, path **e** (as mentioned in Subsection 3.3) is substantially a "dead end" path leading to a bicyclic structure that is located 2.6 kcal $mol^{-1}$ above *exo-axial* $^1$**DZ** and with a denitrogenation channel "locked" by an 8 kcal $mol^{-1}$ barrier. Thus, the bicyclic intermediate will most likely return back to the *exo-equatorial* $^1$**DZ**. Accordingly, although triplet DFT cannot describe the formation of such bicyclic intermediate this force field seems to constitute the best compromise for trajectory computations. Of course, at this level the production and back decomposition of the bicyclic intermediate will not be seen but must be "replaced" an oscillation in the same direction.

In Figures 10 and 11, we report the result of two trajectory computations that differ in the initial conditions. In the first trajectory (Figure 10), we relax the structure from point I without initial kinetic energy. Thus, the relaxation is fully driven by the ground state potential energy surface. It can be clearly seen that the first half-oscillation corresponds to a displacement toward the bicyclic intermediate. In fact both the C1−N2−N1

***Scheme 4***

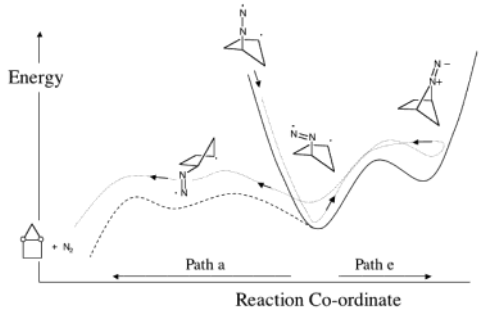


bending and the C4- - -N2 distance are decreased. After 40 fs, the molecule reaches a highly strained structure and starts to relax back thus inverting the initial direction of motion. Within 60 fs, the structures has reached the *exo-axial* $^1$**DZ** configuration and after 80 fs the axial-to-equatorial transition structure. The inverted configuration is then reached in 100 fs. As apparent from Figure 10, the process of axial-to-equatorial inversion of the $^1$**DZ** intermediate occurs impulsively and takes two oscillations along the ground state potential energy surface to be achieved. By continuing the same trajectory one clearly see that within an additional oscillation the N2 moiety is extruded from the *exo-axial* $^1$**DZ** configuration with a clear $S_H2$ process that leads to an *inverted* housane-like cyclopentadiyl radical configuration. Notice that given the fact that the *exo-axial* $^1$**DZ** intermediate only exists for half oscillation (i.e. 50 fs) the trajectory strongly *support the concept of a far from equilibrium (i.e. non statistical)* $^1$***DZ*** *intermediate driving the reaction.*

In Figure 11, we present a second trajectory that has a nonzero initial kinetic energy. In fact, as specified above a velocity vector accounting for the momentum gained during excited-state relaxation has been added to trajectory starting point (i.e. to structure **I**). It can be seen that the general behavior of this second trajectory is very similar. Population of path **a** and inversion is still achieved within three oscillations and with the same time scale. The only remarkable difference is related to the N2 extrusion that begins earlier. In fact, it is apparent that axial-to-equatorial inversion and nitrogen extrusion occurs simultaneously. This means that according to this trajectory an *exo-equatorial* $^1$**DZ** configuration is never achieved but an *inverted* housane-like cyclopentadiyl radical configuration is directly produced in ca. 100 fs.

In conclusion, the mechanism suggested by the two trajectories is that of an impulsively highly coupled ground-state relaxation and inversion. In mechanistic terms this leads to population of path **a**. Nevertheless, one must notice that the first oscillation is not in the direction of path **a** but rather in the direction of path **e** leading to an unstable (transient) bicyclic intermediate. As commented above, the "true" CASPT2 trajectory may display production and reopening of the bicyclic intermediate within the first oscillation. In any case, the trajectory is not likely to remain trapped in the bicyclic well for more than a few oscillations. The final mechanism supported by our computations is reported in Scheme 4 below.

The vibrational motion which connects path **a** and path **e** during the first two oscillations of Figures 10 and 11 can also be understood in terms of population of a specific vibrational mode of the *exo-axial* $^1$**DZ**. In fact vibrational frequency analysis documents the existence of a low frequency (∼100 $cm^{-1}$)

*Scheme 5*

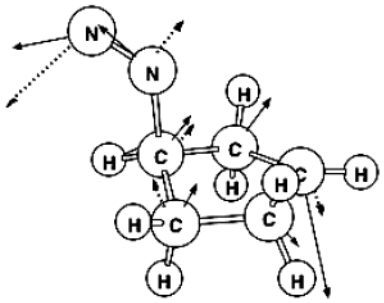

*exo-axial* **$^1$DZ**

normal mode that correlates with such oscillatory motion. The geometrical displacement associated with the mode is presented in Scheme 5. It is apparent from the Scheme that in the positive direction the structure is displaced in the axial-to-equatorial direction, whereas in the negative direction the structure is displaced toward the bicyclic structure**.** The full and dashed arrows in Scheme 5 indicate that such mode is found at both the CASSCF and DFT levels, respectively. It is straightforward that the initial population of this mode corresponds to the generation of a highly nonstatistical *exo-axial* **$^1$DZ** intermediate consistently with the Carpenter model[3].

**3.5 Comparison with the Experimental Results.** The computed (at the CASPT2 level) 0−0 excitation energy of **DBH** is 85.1 kcal mol$^{-1}$ and compares well with the experimentally observed quantity of 84.5 kcal mol$^{-1}$.[24] A second computed quantity that matches the experimental observation is the $^1$n-$\pi$* lifetime of ca. 2 ns for **DBH**,[25] which we assume to be controlled by the singlet α-cleavage barrier (see also Figure 5). In fact, the use of the Arrhenius equation and by assuming an activation entropy of 0.0 kcal mol$^{-1}$ K$^{-1}$ at 298 K, the 5.7 kcal mol$^{-1}$ computed barrier yields a lifetime of 2.4 ns. The computed α-cleavage barrier is of the same magnitude (ca. 3.3 kcal mol$^{-1}$) as observed for a **DBH** derivative in solution.[26] The energetics of the **$^1$DR** region (ca. 14 kcal mol$^{-1}$ stabilization of the *$C_2$-symmetric* **$^1$DR** relative to the **$^1$DZ** diradical and a cyclization barrier of 1.3 kcal mol$^{-1}$ for the **$^1$DR** species) is in agreement with that previously reported by Carpenter and coworkers for the thermal denitrogenation of **DBH**.[3] These authors have shown that the computed energetics is consistent with the experimental enthalpy data.[27]

The good correspondence between the experimental and computed data validates the strategy (see Section 2) used to compute the reaction pathways of Scheme 2. In the following, we shall focus on the qualitative mechanistic aspects of these computed pathways with reference to the stereochemical consequences.

**3.5.1 Singlet Photochemical Route to Housane.** As mentioned above, the mechanistic model that may be extracted from the computational results is centered on the fact that ca. 50 kcal mol$^{-1}$ excess energy will populate, upon excited-state relaxation, only certain vibrational modes. Thus, in the absence of large ground-state barriers, the reaction coordinates dominated by these modes will be impulsively populated. For the parent singlet n-$\pi$*-excited **DBH**, we have provided computational evidence that the favored trajectory for the prevalent production of inverted housane populates path **a**. On the other hand, path **b** affords a 1:1 mixture of inverted and retained housanes, and path **d** leads preferentially to retained housane. The paths **c** and **e** are unproductive for housane production, and will be accessed at a slower rate and on the time scale of thermal equilibration. We conclude that the actual inverted/retained housane ratio and, therefore, the observed extent of stereoselectivity, depends on how effectively the varies paths **a**, **b**, and **d** are populated. It is important to note that a dynamic (nonstatistical) effect is essential to explain the inversion stereochemistry, because the total barrier along path **a** (2.7 kcal mol$^{-1}$) is larger than the barriers for the path **b** (2.0 kcal mol$^{-1}$) and path **d** (3.6 kcal mol$^{-1}$).

Reaction-coordinate analysis demonstrates that $N_2$ departure along all singlet-excited pathways does not involve any significant contribution from the N2−N3 stretching and C1−N2−N3 bending modes that would result in vibrational and rotational excitation of the departing $N_2$ molecule (see for instance the coordinate of path **a** in Figure 6 and path **d** in Figure 3). Analysis of the final parts of the trajectories reported in the previous subsection confirms this idea (see also the Supporting Information). This fact provides a possible explanation for the lack of vibrational and rotational excitation of $N_2$ in the photolysis of the parent **DBH**.[25,28]

An additional experimental observation that calls for an explanation is the ca. unit quantum yield measured for parent **DBH** photolysis.[24] This experimental fact implies that path **c** is not populated during the photolysis, which is consistent with a nonstatistical model, and signifies that the rate of population of the other reactive pathways is higher than the rate of vibrational-energy redistribution. Because the barrier for path **c** only requires ca. 1 kcal mol$^{-1}$, the *exo-axial* **$^1$DZ** structure must be subject to a highly nonstatistical energy distribution (dynamically controlled reactivity) to account for the observed ca. unit quantum yield for the **DBH** denitrogenation. In the past, this type of behavior has been demonstrated for the tetramethylene diradical by using time-resolved experiments.[29] In such experiments, *syn*-tetramethylene was generated by photochemical decomposition of cyclopentanone as precursor. It was shown that ring closure and fragmentation of the intermediate occur on a 700-fs time scale and, thus, take place faster or concurrently with vibrational-energy redistribution. In analogy with the tetramethylene diradical, the *exo-axial* **$^1$DZ** intermediate may populate the $S_H2$ path faster than torsional deformation along path **c**. Furthermore, a subpicosecond lifetime for the **$^1$DZ** diradical would also explain the demonstrated difficulty to detect or trap this intermediate. The trajectory computation seen in the previous suggests a less than 200-fs time scale for the disappearance of the **$^1$DZ** diradical.

(24) Solomon, B. S.; Thomas, T. F.; Steel, C. *J. Am. Chem. Soc.* **1968**, *90*, 2249.
(25) Adams, J. S.; Weisman, R. B.; Engel, P. S. *J. Am. Chem. Soc.* **1990**, *112*, 9115−9121.
(26) Adam, W.; Nau, W. M.; Sendelbach, J.; Wirtz, J. *J. Am. Chem. Soc.* **1993**, *115*, 12 571−12 572. Adam, W.; Nau, W. M.; Sendelbach, J. *J. Am. Chem. Soc.* **1994**, *116*, 7049−7054.
(27) Engel, P. S.; Melaugh, R. A.; Mansson, M.; Timberlake, J. W.; Garner, A. W.; Rossini, F. D. *J. Chem. Thermodyn.* **1976**, *8*, 607−621. Cohen, S. G.; Zand, R.; Steel, C. *J. Am. Chem. Soc.* **1961**, *83*, 2895−2900. Goodman, J. L.; Herman, M. S. *J. Am. Chem. Soc.* **1988**, *110*, 2681−2683. Baldwin, J. E.; Ollerenshaw, J. *J. Org. Chem.* **1981**, *46*, 1−7. Roth, W. R.; Adamczak, O.; Breuckmann, R.; Lennartz, H.-W.; Boese, R. *Chem. Ber.* **1991**, *124*, 2499−2521.
(28) Adams, J. S.; Burton, K. A.; Andrews, B. K.; Weisman, R. B.; Engel, P. S. *J. Am. Chem. Soc.* **1986**, *108*, 7935−7938.
(29) Pedersen, S.; Herek, J. L.; Zewail, A. H. *Science* **1994**, *266*, 1359−1364.

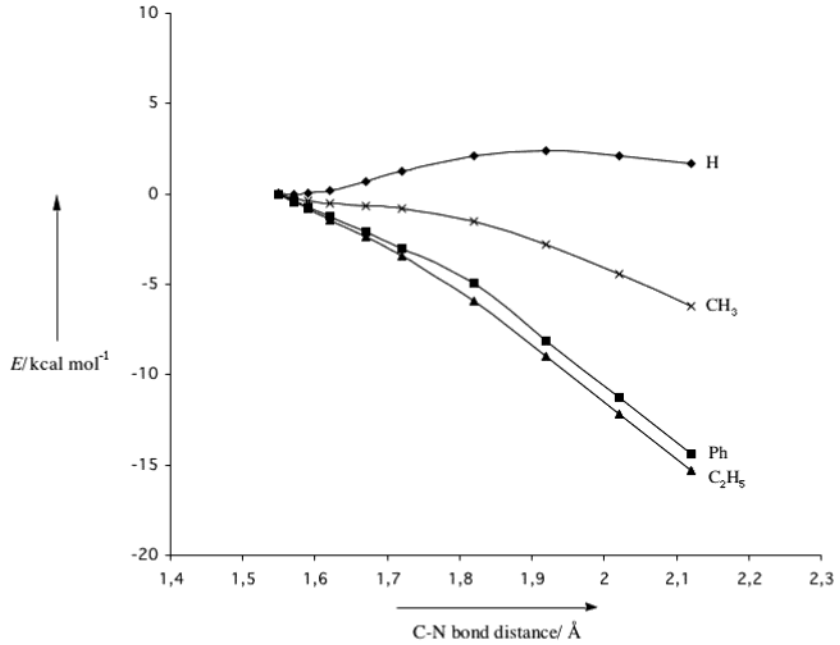


***Figure 12.*** CASPT2 energy profiles for the denitrogenation of the parent (full diamonds) *exo-axial* **$^1$DZ** intermediate and its derivatives with methyl (crosses), ethyl (full triangles) and phenyl (full squares) substituents at one of the bridgehead positions.

**3.5.2 Triplet Photochemical Route to Housane.** An observation that seems in line with the above mechanistic picture concerns the fact that triplet photolysis of parent **DBH** leads to a 1:1 mixture of inverted and retained housanes. In previous work, we have shown that the triplet diradical **$^3$DZ** may be generated by efficient $^1$n-$\pi^*$ to $^3\pi-\pi^*$ intersystem crossing to yield two different types of triplet **DBH** intermediates.[6] A long-lived intermediate with mixed $^3$n-$\pi^*/^3\pi-\pi^*$ character and a short-lived one with exclusive $^3$n-$\pi^*$ character (a transient species with a 25-ns lifetime observed during direct gas-phase photolysis of **DBH** has been assigned to the long-lived intermediate). Both excited states of **DBH** lead to the **$^3$DZ** species by two different α-cleavage pathways. Although the **$^3$DZ** triplet diradical may initially evolve along reaction pathways similar to paths **a**−**d** (Scheme 2), its triplet nature prevents fast housane formation, because intersystem crossing is required, which is relatively slow (nanoseconds) compared to energy redistribution. Although the **$^3$DZ** intermediate may denitrogenate to the **$^3$DR** diradical, the latter will also have to undergo intersystem crossing to its singlet state before ring closure to the housane may occur. The relatively long (nanoseconds) time necessary for intersystem crossing allows for complete thermal equilibration of the **$^3$DR** species to yield its lowest-energy *$C_2$-symmetric* conformer, with the consequence that a 1:1 mixture of the inverted and retained housanes are expected, as experimentally observed.[30]

**3.5.3 Medium Effects on the Ratio of Inverted/Retained Housanes.** The effect of solvent viscosity on the inversion stereochemistry has been recently investigated in the photolysis of ***exo-d$_2$*-DBH**.[9] It was shown that the increase in medium viscosity results in a decrease of stereoselectivity. Also, this viscosity effect may be qualitatively rationalized within the mechanistic scenario discussed above. The viscous medium decreases the efficiency of the impulsive factor and, in turn, the population of path **a** (Scheme 2). At the molecular level, this behavior derives from the fact that the axial-to-equatorial conformational change in the **$^1$DZ** diradical needed for the production of inverted housane involves a large geometrical displacement, which is controlled by a relatively large (2.7 kcal mol$^{-1}$) barrier. Under such conditions, the frictional forces of a viscous media will strongly oppose the motion and, thus, effectively diminish the impulsive population (see previous subsection) along path **a**. This viscosity behavior appears to be quite general, because it has been demonstrated in a highly alkylated **DBH** such as the *syn*-2,3-diaza-4,7-dimethyl-1-ethylbycyclo[2.2.1]heptene, in which both bridgehead positions and the methylene bridge bear substituents.[9]

**3.5.4 Substituent Effects on the Ratio of Inverted/Retained Housanes.** According to Scheme 2, the only way to achieve preferential formation of retained housane, that is, opposite to the inversion stereoselectivity observed in the parent **DBH** photolysis, is through path **d**. Such a preferred retention would constitute a stereochemical memory effect, in which the original configurations at the two bridgehead centers of **DBH** are retained during photolysis. According to Scheme 2, three conditions must be met to achieve efficient retention: (i) Denitrogenation must be made more facile in order to populate efficiently path **d**; (ii) the impulsive motion for the population of path **a** must be restrained, e.g., by increasing the medium viscosity, as seen above, or by strategically placed substituents; (iii) the **$^1$DR** ring motion from the "native" puckered *$C_s$-like* to the lower-energy *$C_2$-symmetric* conformation of the **$^1$DR** species must be retained.

In Figure 12, we show the effect of bridgehead substituents of different size (methyl, ethyl and phenyl) on the strength of the C1−N2 bond for the corresponding putative *exo-axial* **$^1$DZ** intermediate. It is evident that all the substituents destabilize the bond and, in turn, the already weakly bound intermediate. The destabilization follows the order H < $CH_3$ < $C_2H_5$ ∼ Ph and relates to the ability of the substituent to stabilize the

(30) Adam, W.; Fragale, G.; Klapstein, D.; Nau, W. M.; Wirz, J. *J. Am. Chem. Soc.* **1995**, *117*, 12 578.

incipient radical center at the C1 position. For the $CH_3$, $C_2H_5$ and Ph substituents we compute no barrier and, thus, the *exo-axial* **$^1$DZ** structure would not exist as a bona fide intermediate for these substituted **DBH** derivatives. Although in these systems, the *formal* existence of a diazenyl diradical intermediate is unlikely (no energy minimum on the potential energy surface), the dynamics imposed by its photochemical generation would still produce transients close in molecular structure to the diazenyl diradical depicted by *exo-axial* **$^1$DZ** structure. We contend that the difference in the behavior of these intrinsically labile transients and a nonstatistical **$^1$DZ** intermediate is nominal. Consequently, bridgehead substitution is one factor that increases the probability of preferentially populating path **d** relative to path **a**. A second factor to diminish the population of path **a** relates to the mass and steric hindrance of the bridgehead substituents. In fact, the efficacy of utilizing the C1−N2−N3 momentum for the impulsive axial-to-equatorial conformational change should depend on the mass that needs to be displaced during the change. Since during the axial-to-equatorial motion the bridgehead substituents experience a substantial displacement, we expect that heavier bridgehead substituents will modify the impulsive motion through an inertial effect and path **a** will be less populated (i.e., according to Scheme 4 the relaxation will stop in the *exo-axial* **$^1$DZ** region). Notice that the same inertia effect may restrain the transformation of the native *$C_s$-like* **$^1$DR** to the more stable *$C_2$-symmetric* conformation.

As discussed above, bridgehead substitution appears to satisfy the conditions i−iii to foster the formation of retained housane. For this reason, we have conducted a detailed experimental investigation of the photolysis of bridgehead-substituted **DBH** derivatives, tailor-made for this purpose. [31] It is shown that the amount of retention increases with the mass of the C1/C4 substituents in the order H/H < H/$CH_3$ < $CH_3$/$CH_3$ < H/Ph < Ph/Ph. Indeed, for the Ph/Ph case, the retained housane is actually the only product obtained after photolysis, that is, perfect *stereochemical* memory. Moreover, the presence of a conformational "lock" such as the annelated five-membered ring at the C5−C6 position of the **DBH** skeleton further detains the *$C_s$-like* to *$C_2$-symmetric* conformational change.

## 4. Conclusions

Our computations indicate that the photochemical denitrogenation of the parent **DBH** occurs by single bond breaking to initially form a diazenyl diradical as intermediate in a $\sigma,\sigma$ electronic configuration. Thus, the mechanism for the photochemical reaction differs from that of the corresponding thermal denitrogenation, which has been recently proposed [3] to involve concerted bond breaking of the two C−N bonds. The computed energetics suggests that a *thermally equilibrated diazenyl diradical* would preferentially produce a *$C_2$-symmetric* singlet cyclopentane-1,3-diyl diradical (path **b**) with exclusive production of a 1:1 mixture of retained and inverted housane, in contrast with the experimental observations. Consequently, we argue that *the experimental results may be explained in terms of a **$^1$DZ** intermediate which reacts before thermal equilibration.*

Intermediates such as the **$^1$DR** *or* **$^1$DZ** diradicals are usually expected to lie in energy minima on the potential energy surface of the reacting system. The intermediate is generated through a reactive event (e.g., the passage through a transition state) that deposits an excess of vibrational energy into a specific mode of the system. Usually, it is assumed that the intermediate remains "trapped" in the corresponding energy well long enough to allow for internal vibrational-energy redistribution (IVR) and thermal equilibration. However, if the energy minimum is located in a flat region of the potential energy surface, its lifetime may be too short to allow for the IVR process. In this case, a nonstatistical (not thermally equilibrated) intermediate results, whose reactivity may be determined by the nature of the vibrationally excited modes rather then by the lowest-energy reaction path. The concerted generation of a nonstatistical *$C_2$-symmetric* **$^1$DR** diradical with at least 8 kcal mol$^{-1}$ excess energy in the ring-inversion mode has been recently proposed to account for the inversion stereoselectivity observed in the *thermal* denitrogenation of the parent **DBH**[3]. The concept of nonstatistical dynamics as a factor in determining the stereoselectivity of thermal reactions has been intensively investigated by Carpenter.[32]

In singlet *photochemical* reactions, intermediates are produced by the decay of excited states at a conical-intersection funnel.[33] Expectedly, in photochemical transformations, the involvement of nonstatistical intermediates is more probable, due to the fact that a larger amount of excess vibrational energy becomes available to activate specific modes. Herein, we have computed that the photolysis of the parent **DBH** yields a diazenyl diradical with ca. 50 kcal mol$^{-1}$ excess vibrational energy. Such an intermediate will be able to overcome a barrier of few kcal mol$^{-1}$, provided that the excess energy populates a mode along the corresponding reaction pathway. The nonstatistical *exo-axial* **$^1$DZ** intermediate has its excess vibrational energy in the modes for ring inversion, ring planarization and CN-bond elongation. Thus, from our computational work we conclude that, similar to the thermolysis, the photolysis of **DBH** may be understood on the basis of a nonstatistical intermediate. However, *this intermediate corresponds to an exo-axial **$^1$DZ** rather then to the $C_2$-symmetric **$^1$DR** intermediate* proposed for the thermal denitrogenation. Because the lifetime of such an intermediate must be shorter than the time required for the IVR process, it is likely that the lifetime of our nonstatistical *exo-axial* **$^1$DZ** transient would fall in the picosecond or even subpicosecond time scale. This explains its experimentally elusive nature, but femtosecond-time-resolved spectroscopy should be able to detect such a putative species. The production of a transient *an exo-axial **$^1$DZ*** intermediate is directly suggested by the classical trajectory computations presented above. This species would live less than few hundred femtoseconds and will invert to *exo-equatorial **$^1$DZ*** long before thermalization.

Our computations disclose that the inversion stereoselectivity observed in the photolysis of the parent **DBH** is related to the specific nature of the impulsively populated vibrational mode that ultimately results in the axial-to-equatorial ring inversion. As pointed out previously in Subsection 3.4 ("Comparison with the Experimental Results"), the efficacy of populating the inversion mode (path **b** in Scheme 2) may be manipulated experimentally through dissipation of the available excess vibrational energy by increasing, for instance, the solvent viscosity (Subsection 3.4.3) or by strategically placed bulky

(31) Adam, W.; García, H.; Diedering, M.; Martí, V.; Olivucci, M.; Palomares, E. *J. Am. Chem. Soc.* **2002**, *124*, 12 192−12 199.

(32) Carpenter, B. K. *Acc. Chem. Res.* **1992**, *25*, 520−528.

(33) Bernardi, F.; Olivucci, M.; Robb, M. A. *Chem. Soc. Rev.* **1996**, *25*, 321−328.

substituents (Subsection 3.4.4). From this point of view, the mechanistic network given in Scheme 2 should serve as a "road map", to be followed for favoring the production of either inverted or of retained housane. In this context, triplet sensitization also offers a means to control the stereochemistry of the photochemical reaction. The longer lifetime (usually nanoseconds) of triplet diradicals ultimately leads to the thermally equilibrated *$C_2$-symmetric* $^3$**DR** intermediate with complete loss of stereoselectivity.

**Acknowledgment.** We are grateful to Prof. B. K. Carpenter for helpful discussions. Generous funds for the work at Siena have been provided by the Università di Siena (Progetto di Ateneo A.A. 00/02), NATO (CRG 950748), and HFSP (RG 0229/2000-M), for the work at Würzburg by the Deutsche Forschungsgemeinschaft, the Volkswagen-Stiftung, and the Fonds der Chemischen Industrie. C.P. and M.O. are grateful for the EU Marie-Curie Grant No. HPMF-CT-1999-00384. We wish to thank the "Swiss Center for Scientific Computing" and "Cineca" for granted calculation time on their computers.

**Supporting Information Available:** The Cartesian coordinates of all structures discussed in the text are given and one table with their CASSCF and CASPT2 energies (14 pages). Two QuickTime movies documenting the computed trajectories are given. This material is available free of charge in the Internet at http://pubs.acs.org.

JA0263137